Hydrology and Earth System Sciences

Influence of infiltration and soil storage capacity on the skewness of the annual maximum flood peaks in a theoretically derived distribution

A. Gioia[1], V. Iacobellis[1], S. Manfreda[2], and M. Fiorentino[2]

[1]Dipartimento di Ingegneria delle Acque e di Chimica, Politecnico di Bari, Bari, Italia
[2]Dipartimento di Ingegneria e Fisica dell'Ambiente, Università degli Studi della Basilicata, Potenza, Italia

Correspondence to: A. Gioia (a.gioia@poliba.it)

Abstract. Understanding the spatial variability of key parameters of flood probability distributions represents a strategy to provide insights on hydrologic similarity and building probabilistic models able to reduce the uncertainty in flood prediction in ungauged basins. In this work, we exploited the theoretically derived distribution of floods model TCIF (Two Component Iacobellis and Fiorentino model; Gioia et al., 2008), based on two different threshold mechanisms associated to ordinary and extraordinary events. The model is based on the hypotheses that ordinary floods are generally due to rainfall events exceeding a constant infiltration rate in a small source area, while the so-called outlier events responsible for the high skewness of flood distributions are triggered when severe rainfalls exceed a storage threshold over a large portion of the basin. Within this scheme, a sensitivity analysis was performed with respect to climatic and geomorphologic parameters in order to analyze the effects on the skewness coefficient and provide insights in catchment classification and process conceptualization. The analysis was conducted to investigate the influence on flood distribution of physical factors such as rainfall intensity, basin area, and particular focus on soil behavior.

1 Introduction

The understanding of processes control on the shape of the flood frequency distribution is essential to extrapolate reliable at-site predictions to large return periods and to define meaningful similarity indicators between catchments for flood frequency estimation in ungauged catchments (Merz

and Bloschl, 2009). These physical interconnections may be explored using an upward approach (or model based), where a stochastic rainfall model is coupled with a runoff model using derived distributions (Eagelson, 1972; Raines and Valdes, 1993; Gottschalk and Weingartner, 1998; Fiorentino and Iacobellis, 2001; De Michele and Salvadori, 2002; Franchini et al., 2005; Bocchiola and Rosso, 2009) or Monte Carlo simulations (e.g. Beven, 1987; Loukas, 2002; Blazkova and Beven, 2002; Fiorentino et al., 2007).

The literature proposes several schemes and procedures for the theoretical derivation of flood probability distributions. Most of the derived distributions developed so far are based on a single runoff generation scheme, but this may represent a limitation in the description of runoff production. Moreover, it is not always clear how well a single component describes the complex dynamics of flood formation within the river basin. In this context, the presence of different runoff generation processes, such as the saturation excess and the infiltration excess, under different climatic conditions and the dynamics which control the transition between the two schemes, may provide interesting insights useful to find similarities and differences among river basins and among their processes for classification and regionalization. Sivapalan et al. (1990) accounted for the effect of different mechanisms of runoff generation (infiltration excess and saturation excess), while Iacobellis and Fiorentino (2000) introduced the partial contributing area as a random variable and considered only one runoff threshold associated to infiltration excess in arid basins or to saturation excess in humid basins.

The effects of runoff thresholds have received particular attention in flood frequency analysis in last few years

(e.g. McGrath et al., 2007). Kusumastuti et al. (2007) focused on catchment storage and derived the flood frequency distributions by Monte Carlo simulations, using a non-linear conceptual rainfall-runoff model. Struthers and Sivapalan (2007) illustrate the impact of heterogeneity associated with threshold nonlinearities in the storage-discharge relationship associated with the rainfall-runoff process upon flood frequency behaviour. They introduced two storage thresholds, namely a field capacity storage and a catchment storage capacity, that identify two different flood frequency "regions". The return period associated with the transition between these regions is directly related to the frequency of threshold exceedance.

Following this line of investigation, this paper describes the effects of different runoff production mechanisms on the generation of ordinary and extraordinary flood events, exploiting the TCIF flood frequency distribution (Gioia et al., 2008). The study analyses the effects of climatic and geomorphologic parameters, with particular focus on soil behaviour, on statistical flood moments and in particular on the skewness coefficient.

Some interesting results in this direction were already obtained by Iacobellis et al. (2002) exploiting the theoretical model proposed by Iacobellis and Fiorentino (2000). In particular, they explored the spatial variability of the coefficient of variation of annual maximum floods. They derived a theoretical dependence between the coefficient of variation (C_v) and the abstraction characteristics at the basin scale, the basin area and rainfall parameters. Their findings highlighted that C_v follows scaling relationships with basin area, with distinct behavior dependent on the dominant runoff mechanism. In particular, C_v decreases with area when the infiltration excess mechanism dominates, while C_v increases with area in humid and vegetated basins where saturation excess runoff takes place.

On the other hand, the skewness coefficient (C_s) can vary vastly in catchments, which apparently exhibit similar flood behaviour (Matalas et al., 1975). This may be due to the interaction of temporal varying observation periods and climate fluctuations, single extreme events and observation errors (Merz and Bloschl, 2009). According to McCuen and Smith (2008), the flood skew estimation involves rainfall skew and watershed and channel storage. In their scheme, rainfall skew represents an upper bound on the population of runoff skew and flood skew decreases from the rainfall skew for the same location as storage increases.

In any case, the spatial variability of C_s plays a crucial role in the hierarchical approach for regional flood frequency analysis (Fiorentino et al., 1987) and is recognized as one of the main factors influencing the estimation of upper quantiles of annual peak flows (e.g. Strupczewski et al., 2011). Indications on the physical controls on this specific parameter is essential for a reliable evaluation of the upper quantiles and for extrapolating at-site statistics to large return periods.

The paper is structured as follows. Section 2 briefly summarizes the main features of the TCIF model. In Sect. 3 the organization and main focus of the sensitivity analysis are explained. In Sect. 4 results of the sensitivity analysis are shown and commented. Section 5 reports conclusions and perspectives of this research.

2 Theoretically derived flood frequency distribution (TCIF model)

The TCIF distribution was derived by Gioia et al. (2008) under the hypothesis that in natural basins different mechanisms of runoff generation may coexist, being in turn responsible of the peak flow, depending on the characteristics of the rainfall event and on the antecedent moisture conditions. Thus, two components arise characterized by:

- L-type (frequent) response, occurring when rainfall intensity ($i_{a,\tau}$) exceeds a lower threshold $f_{a,L}$, and responsible of ordinary floods likely produced by a relatively small portion of the basin a_L; the L-type (frequent) peak unit runoff is: $u_{a,L} = \xi(i_{a,\tau} - f_{a,L})$.

- H-type (rare) response, occurring when rainfall intensity exceeds a higher threshold $f_{a,H}$, and providing extraordinary floods mostly characterized by larger contributing areas a_H; the H-type (rare) peak unit runoff is: $u_{a,H} = \xi(i_{a,\tau} - f_{a,H})$.

Other assumptions of the TCIF distribution model are that rainfall and infiltration, averaged in space and time, scale with the contributing area with the following relationships:

$$E[i_{a,\tau}] = I_1 \, a^{-\varepsilon} = E[i_{A,\tau}] \, (a/A)^{-\varepsilon} \tag{1}$$

$$f_{a,L} = f_{A,L} \, (a_L/A)^{-\varepsilon_L} \tag{2}$$

$$f_{a,H} = f_{A,H} \, (a_H/A)^{-\varepsilon_H}. \tag{3}$$

The rainfall intensity is considered Weibull distributed (with shape parameter k) and the contributing areas a_L and a_H have a continuous part, Gamma distributed, and a spike of discrete probability for $a = A$ total basin area. These distributions are characterized by a parameter β which depends on the coefficient of variation and is assumed constant. Other parameters are $\alpha_L = r_L A/\beta$ and $\alpha_H = r_H A/\beta$ which depend on the mean value, once the β value is fixed, being the mean value represented by the dimensionless parameters $r_L = E[a_L]/A$ and $r_H = E[a_H]/A$ with $r_H \geq r_L$.

Assuming that L-type and H-type events are independent and that both rates of occurrence are Poisson distributed, the overall process of exceedances is also a Poisson process, and the following relationships hold:

$$\Lambda_H = \Lambda_p \exp\left(-\frac{f_{A,H}^k}{E[i_{A,\tau}^k]}\right) \tag{4}$$

and

$$\Lambda_q = \Lambda_L + \Lambda_H = \Lambda_p \exp\left(-\frac{f_{A,L}^k}{E\left[i_{A,\tau}^k\right]}\right). \qquad (5)$$

Λ_L and Λ_H are the mean annual number of independent flood events for the L-type and the H-type events.

In compound Poisson processes, if the base process of rainfall intensity follows the exponential distribution, then the annual maximum rainfall intensity is Gumbel distributed. The exponential distribution corresponds to a Weibull distribution with $k = 1$. Then, in this case, we may write:

$$E\left[i_{A,\tau}^k\right] = E\left[i_{A,\tau}\right] = I_A = I_1 A^{-\varepsilon} \qquad (6)$$

with I_1 the rainfall intensity per unit contributing area and ε a scaling coefficient dependent on the slope of the areal rainfall IDF (intensity duration frequency) curves.

The general expression of the cumulative probability distribution of the annual maximum flood peak and its probability density function are reported in Iacobellis et al. (2011). In the particular case of rainfall intensity exponentially distributed, the cumulative probability distribution, $\text{CDF}_{Q_p}(q_p)$, of the annual maximum flood peak $q_p = Q + q_o$, with q_o the base flow, and its probability density function become:

$$\text{CDF}_{Q_p}(q_p) = \exp\left\{-\Lambda_L\left[\int_0^A g\,(a_L)\,\exp\right.\right.$$

$$\left.\left(-\frac{(q_p - q_o)/(\xi\,a_L)}{E\left[i_{a_L,\tau}\right]}\right)\right]\,\mathrm{d}\,a_L\right\}\cdot\exp$$

$$\left\{-\Lambda_H\left[\int_0^A g\,(a_H)\,\exp\left(-\frac{(q_p - q_o)/(\xi\,a_H)}{E\left[i_{a_H,\tau}\right]}\right)\,\mathrm{d}\,a_H\right]\right\} \qquad (7)$$

$$\text{PDF}_{Q_p}(q_p) = \text{CDF}_{Q_p}(q_p)\left[\Lambda_L\left\{\int_0^A g\,(a_L)\right.\right.$$

$$\frac{1}{(\xi\,a_L)\,E\left[i_{a_L,\tau}\right]}\exp\left(-\frac{(q_p - q_o)/(\xi\,a_L)}{E\left[i_{a_L,\tau}\right]}\right)\,\mathrm{d}a_L\right\}$$

$$+\Lambda_H\left\{\int_0^A g\,(a_H)\,\frac{1}{(\xi\,a_H)\,E\left[i_{a_H,\tau}\right]}\right.$$

$$\left.\left.\exp\left(-\frac{(q_p - q_o)/(\xi\,a_H)}{E\left[i_{a_H,\tau}\right]}\right)\,\mathrm{d}\,a_H\right\}\right]. \qquad (8)$$

$E[i_{a_L,\tau}]$ and $E[i_{a_H,\tau}]$ are, respectively, the average rainfall intensity with respect to contributing areas a_L and a_H, ξ is a constant routing factor, $g(a_L)$ and $g(a_H)$ are, respectively, the probability density functions of the L-type and H-type contributing areas.

3 Methodology and organization of the sensitivity analysis

In Gioia et al. (2008) and Iacobellis et al. (2011), particular attention was paid to the dynamics of runoff source areas by revealing the scaling behaviour of the runoff thresholds ($f_{A,L}$ and $f_{A,H}$). In particular, investigating the different mechanisms of runoff production that coexist in different climates, they found that the scaling behaviour of the H-type (rare events) runoff threshold corresponds to a storage threshold associated to a mechanism of infiltration excess. This kind of response arises when an intense and persistent rainfall of significant areal extension exceeds a water storage capacity over large and more or less vegetated hillslopes. On the other hand, the L-type (frequent events) runoff threshold corresponds to a constant (and low) infiltration rate associated to a saturation excess mechanism.

In order to keep trace of the different role of infiltration rate and soil storage capacity and soil storage capacity in the proposed sensitivity analysis, we characterize the two runoff thresholds considering the lower threshold $f_{A,L}$ as associated to the spatial average of a constant soil infiltration rate in saturated conditions, ϕ,

$$f_{A,L} \cong \phi. \qquad (9)$$

Then, we consider the soil water storage capacity averaged in space and over the basin lag-time, which scales with basin area as:

$$W_A = W_1 A^{-0.5}; \qquad (10)$$

the higher runoff threshold can be evaluated as:

$$f_{A,H} \cong \phi + W_A. \qquad (11)$$

When rainfall exceeds the lower threshold, a small source area a_L corresponding to the first (L-type) component is activated with mean annual number of exceedances equal to $\Lambda_q = \Lambda_H + \Lambda_L$ (see Eq. 5). The exceedances of the second runoff threshold characterize the activation of a larger source area a_H corresponding to the second (H-type) component with mean annual number of exceedances equal to Λ_H (see Eq. 4).

In order to provide a general framework for the physical interpretation of results, in Table 1 we consider the range of variability of each threshold parameter (ϕ and W_A) divided in three classes: low, medium and high. Then, a qualitative evaluation of the occurrences of the two different components is derived from Eqs. (4) and (5). In fact, the occurrence of events of the 1st and 2nd components is related to the probability of rainfall to exceed the corresponding thresholds. For each cell of Table 1, we indicate in the upper left corner the frequency of the L-type component, corresponding to the probability $P(i > \phi)$, and in the bottom right corner the frequency of the H-type component, corresponding to the probability $P(i > \phi + W_A)$. Thus, for low values of

Table 1. Frequency of rainfall exceedance over different thresholds ϕ and W_A.

| Constant infiltration rate (ϕ) | $P(i > \phi)$ / $P(i > W_A + \phi)$ | Soil storage capacity (W_A) | | |
		Low	Medium	High
Low	$P(i > \phi)$	frequent	frequent	frequent
	$P(i > W_A + \phi)$	frequent	occasional	rare
Medium	$P(i > \phi)$	occasional	occasional	occasional
	$P(i > W_A + \phi)$	occasional	rare	very rare
High	$P(i > \phi)$	rare	rare	rare
	$P(i > W_A + \phi)$	rare	very rare	extremely rare

Table 2. Expected basin behaviour, in terms of presence and weight of the two components, based on a broad classification of the different thresholds ϕ and W_A.

| Constant infiltration rate (ϕ) | CDF type | Soil storage capacity (W_A) | | |
		Low	Medium	High
	Low	1 component	2 components (1st may be not relevant)	2 components (1st may be not relevant)
	Medium	1 component (both are relevant)	2 components (2nd may be not observed)	2 components
	High	1 component (2nd may be not observed)	2 components (2nd may be not observed)	2 components

the constant infiltration rate at saturation ϕ, the probability of rainfall to exceed the first runoff threshold is high; for increasing ϕ values, the number of rainfall events that exceeds the first runoff threshold becomes occasional for medium ϕ and rare for high ϕ. Then, if the storage capacity W_A assumes values belonging to the lower class, the occurrence of exceedances of the second runoff threshold is frequent, occasional and rare, as it is in the range of variation of the constant infiltration rate ϕ (first column in Table 1); for a medium value of ϕ, the occurrence of the exceedances is occasional, rare, and very rare (second column in Table 1), and for high ϕ value it becomes rare, very rare, and extremely rare (third column in Table 1).

Following the above arguments, we report in Table 2 the expected behaviour of a basin regime in terms of presence and relevance of the two runoff components. For low values of the soil storage (W_A), the two runoff thresholds are close (see Eqs. 9 and 11); then, it is possible to recognize only one component (L-type) of the theoretical model (first column of Table 2). When soil storage increases the second component may become distinguishable; in particular for medium values of the soil storage, the first component may be not relevant to the right tail of the flood frequency curve if the constant infiltration rate ϕ is low (only the H-type component is present). On the other hand, if ϕ is high the second runoff threshold assumes very high values; then the second component may become not observable. Even for high values of soil storage, with increasing the values of ϕ, the frequency of exceedances of the second runoff threshold will be so low that the second component may be not observable and not significant for return periods of technical interest. It happens that only for medium values of both ϕ and W_A, the two components are both relevant to the right tail of the flood frequency curve.

In order to investigate the role that the combination of the two processes may have on the shape of the flood frequency curve, the sensitivity analysis was carried out changing the rate of L-type and H-type events over a broad range that embraces all possible cases identified above. Those values, given only qualitatively in Tables 1 and 2, are provided in Table 3 in terms of mean annual number of flood events Λ_q,

Table 3. Mean annual number of events of the 2nd component (H-type response) based on different values of Λ_Q and Λ_H/Λ_Q.

		Λ_H					
Λ_Q		Λ_H/Λ_Q					
		1/3	1/10	1/20	1/50	1/200	1/1000
High	20	6.667	2.000	1.000	0.400	0.100	0.020
Medium	10	3.333	1.000	0.500	0.200	0.050	0.010
Low	5	1.667	0.500	0.250	0.100	0.025	0.005

Table 4. Values of dimensionless ratios ϕ/I_A (for $\Lambda_p = 21$) and W_A/I_A, based on different values of Λ_q and Λ_H/Λ_q.

		ϕ/I_A					
$\Lambda_p = 21$		Λ_H/Λ_q					
Λ_q		1/3	1/10	1/20	1/50	1/200	1/1000
High	20	0.049	0.049	0.049	0.049	0.049	0.049
Medium	10	0.742	0.742	0.742	0.742	0.742	0.742
Low	5	1.435	1.435	1.435	1.435	1.435	1.435
		W_A/I_A					
Λ_q		Λ_H/Λ_q					
		1/3	1/10	1/20	1/50	1/200	1/1000
High	20	1.099	2.303	2.996	3.912	5.298	6.908
Medium	10	1.099	2.303	2.996	3.912	5.298	6.908
Low	5	1.099	2.303	2.996	3.912	5.298	6.908

equal to the number of rainfall events that exceed the first threshold ϕ, and the average annual number of flood events Λ_H exceeding also the second threshold $W_A + \phi$. According to the variability of Λ_q observed in Southern Italy (see Iacobellis et al., 2011), we considered values of 5, 10 and 20 flood events per year as representative of, respectively, low, medium and high frequency. For the occurrence of the second runoff threshold we considered six values obtained by adopting a fixed ratio between the mean annual number of occurrences Λ_H and Λ_q (1/3, 1/10, 1/20, 1/50, 1/200 and 1/1000).

Under the hypothesis of rainfall intensity exponential distributed, with $k = 1$, and replacing Eqs. (6) and (11) in Eq. (4) we obtain:

$$\frac{\phi + W_A}{I_A} = -\ln\left(\frac{\Lambda_H}{\Lambda_p}\right). \tag{12}$$

Replacing Eqs. (6) and (9) in Eq. (5), we obtain:

$$\frac{\phi}{I_A} = -\ln\left(\frac{\Lambda_q}{\Lambda_p}\right); \tag{13}$$

and combining Eqs. (12) and (13), we obtain:

$$\frac{W_A}{I_A} = -\ln\left(\frac{\Lambda_H}{\Lambda_q}\right). \tag{14}$$

Following Eq. (14), the ratio Λ_H/Λ_q depends only on W_A/I_A. Moreover, following Eqs. (12) and (13), for a fixed value of Λ_p, Λ_q depends only on the ratio ϕ/I_A, and Λ_H depends only on the ratio $(\phi + W_A)/I_A$. Therefore, for a fixed value of Λ_p, of the ratio Λ_H/Λ_q and of Λ_q it is possible to calculate the corresponding values of ϕ/I_A and W_A/I_A. In Table 4 we report the values of the dimensionless ratios ϕ/I_A obtained by means of Eq. (13), for $\Lambda_p = 21$ and different values of Λ_q and Λ_H. Table 4 reports also the values of the dimensionless ratio W_A/I_A obtained by means of Eq. (14) for different values of Λ_q and Λ_H. In both cases the corresponding values of Λ_H are those reported in Table 3 for the same Λ_q-row and Λ_H/Λ_q-column. For known values of ϕI_A and W_A/I_A, ϕ and W_A can be obtained according to values of I_1, A and ε, which, following Eq. (6), provide I_A. Other parameters affecting the TCIF cumulative distribution function in Eq. (7) are the ratios of the average contributing areas r_L and r_H during a L-type and H-type event, respectively.

The sensitivity analysis was performed by numerically evaluating the TCIF cumulative distribution function and its probability density function, $\text{PDF}_{Qp}(q_p)$, for different sets of parameters Λ_p, I_1, ε, A, r_L, r_H, Λ_H/Λ_q and Λ_q, and keeping constant the values of the following other parameters:

- the routing factor ξ assumed equal to 0.7, as in Iacobellis and Fiorentino (2000);

- the shape parameter β of the gamma distribution of the contributing areas assumed equal to 4, as in Iacobellis and Fiorentino (2000);

- the exponents ε_L and ε_H of the power law relationship between infiltration losses and contributing area assumed, respectively, equal to 0 and 0.5, as reported in Gioia et al. (2008). The skewness coefficient of the distribution was evaluated by numerically solving the equation:

$$C_s = \frac{\int_{-\infty}^{+\infty} (q_p - \mu(q_p))^3 \, \text{PDF}_{Q_p}(q_p) \, dq_p}{\left[\int_{-\infty}^{+\infty} (q_p - \mu(q_p))^2 \, \text{PDF}_{Q_p}(q_p) \, dq_p\right]^{3/2}};$$

$$\text{with} \quad \mu(q_p) = \int_{-\infty}^{+\infty} q_p \, \text{PDF}_{Q_p}(q_p) \, dq_p. \tag{15}$$

In order to provide a structured analysis of the influence of physical factors such as soil infiltration rate at saturation and soil storage capacity on the TCIF distribution and its skewness, the values of Λ_H and Λ_q were selected on the basis of Table 3, hence, for fixed values of the ratio Λ_H/Λ_q. Then, in order to analyze the roles of ϕ and W_A, we used the ratios ϕ/I_A and W_A/I_A shown in Table 4.

For the other parameters of the TCIF distribution, we assigned a range of variability coherent with observed values

www.hydrol-earth-syst-sci.net/16/937/2012/

Hydrol. Earth Syst. Sci., 16, 937–951, 2012

Table 5. Mean and standard deviation of skewness for $r_L = 0.1$, $r_H = 0.3$; A ranges from 10 to 500 km^2 and I_1 ranges from 10 to 50 mm h^{-1}.

	Mean of skewness					
	$W_A/I_A = 1.098$	$W_A/I_A = 2.302$	$W_A/I_A = 2.996$	$W_A/I_A = 3.912$	$W_A/I_A = 5.298$	$W_A/I_A = 6.908$
$\phi/I_A = 0.049$	1.858	2.252	2.260	2.053	1.743	1.612
$\phi/I_A = 0.742$	1.999	2.324	2.248	1.995	1.714	1.608
$\phi/I_A = 1.435$	2.225	2.452	2.308	2.039	1.792	1.707
	Standard deviation of skewness					
	$W_A/I_A = 1.098$	$W_A/I_A = 2.302$	$W_A/I_A = 2.996$	$W_A/I_A = 3.912$	$W_A/I_A = 5.298$	$W_A/I_A = 6.908$
$\phi/I_A = 0.049$	0.025	0.066	0.082	0.077	0.049	0.034
$\phi/I_A = 0.742$	0.017	0.038	0.038	0.021	0.006	0.016
$\phi/I_A = 1.435$	0.011	0.018	0.010	0.009	0.028	0.035

Table 6. Mean and standard deviation of skewness for $r_L = 0.1$, $r_H = 0.6$; A ranges from 10 to 500 km^2 and I_1 ranges from 10 to 50 mm h^{-1}.

	Mean of skewness					
	$W_A/I_A = 1.098$	$W_A/I_A = 2.302$	$W_A/I_A = 2.996$	$W_A/I_A = 3.912$	$W_A/I_A = 5.298$	$W_A/I_A = 6.908$
$\phi/I_A = 0.049$	1.595	2.268	2.832	3.124	2.565	1.858
$\phi/I_A = 0.742$	1.820	2.720	3.127	3.151	2.385	1.786
$\phi/I_A = 1.435$	2.188	3.155	3.417	3.172	2.325	1.837
	Standard deviation of skewness					
	$W_A/I_A = 1.098$	$W_A/I_A = 2.302$	$W_A/I_A = 2.996$	$W_A/I_A = 3.912$	$W_A/I_A = 5.298$	$W_A/I_A = 6.908$
$\phi/I_A = 0.049$	0.011	0.233	0.060	0.102	0.108	0.057
$\phi/I_A = 0.742$	0.008	0.028	0.048	0.066	0.040	0.004
$\phi/I_A = 1.435$	0.007	0.023	0.035	0.035	0.002	0.028

on a set of river basins in Southern Italy investigated in previous studies (Gioia et al., 2008; Fiorentino et al., 2011; Iacobellis et al., 2011). In particular, the mean annual number of rainfall events Λ_p ranges from 21 to 75 (event/year), the rainfall intensity per unit of contributing area I_1 varies from 10 to 50 mm h^{-1}, the basin area A ranges from 10 to 500 km^2; the rainfall scaling coefficient ε varies from 0.3 to 0.4; and the ratios of mean contributing area r_L and r_H range from 0 to 1 with $r_H >= r_L$. We first report results for the entire observed variability of r_L, r_H, basin area A and rainfall intensity I_1 and for the fixed values $\Lambda_p = 21$ and $\varepsilon = 0.3$. Significant results obtained for different values of Λ_p and ε are also discussed, provided that changing these last two parameters does not affect qualitatively the results and their implications on the paper focus, which is the understanding of the role of soil infiltration rate at saturation and soil storage capacity on the presence of two runoff components and on the flood distribution skewness. We did not introduce any change of parameters ξ and β because in all the applications performed on real cases in previous studies

they did not show any variability. In the present application, the base flow q_o is set to zero, because in the TCIF model, q_o is added as a constant factor to the peak flow and hence does not affect the peak flow distribution. Finally, the analysis does not account for changes in the shape parameter k of the rainfall pdf (i.e. of rainfall skewness), which is left to further research.

4 Results and discussion

Results of the sensitivity analysis are described in the present section with particular emphasis on the skewness coefficient of the theoretical distributions. Results are reported in the form of growth curve probability plots and summarized in tabular form (see Tables 5–9).

According to the index flood method (NERC, 1975), the growth curve represents, by definition, the cdf of the growth factor

$$K_x = x/E[x], \tag{16}$$

Table 7. Mean and standard deviation of skewness for $r_L = 0.3$, $r_H = 0.6$; A ranges from 10 to 500 km^2 and I_1 ranges from 10 to 50 mm h^{-1}.

|	Mean of skewness					
	$W_A/I_A = 1.098$	$W_A/I_A = 2.302$	$W_A/I_A = 2.996$	$W_A/I_A = 3.912$	$W_A/I_A = 5.298$	$W_A/I_A = 6.908$
$\phi/I_A = 0.049$	1.562	1.638	1.615	1.578	1.549	1.540
$\phi/I_A = 0.742$	1.645	1.695	1.662	1.621	1.591	1.582
$\phi/I_A = 1.435$	1.805	1.826	1.785	1.741	1.712	1.703
	Standard deviation of skewness					
	$W_A/I_A = 1.098$	$W_A/I_A = 2.302$	$W_A/I_A = 2.996$	$W_A/I_A = 3.912$	$W_A/I_A = 5.298$	$W_A/I_A = 6.908$
$\phi/I_A = 0.049$	3.38E-03	6.21E-03	7.23E-03	7.99E-03	8.39E-03	8.51E-03
$\phi/I_A = 0.742$	2.67E-03	4.56E-03	5.18E-03	5.63E-03	5.86E-03	5.92E-03
$\phi/I_A = 1.435$	1.93E-03	3.15E-03	3.49E-03	3.72E-03	3.78E-03	3.83E-03
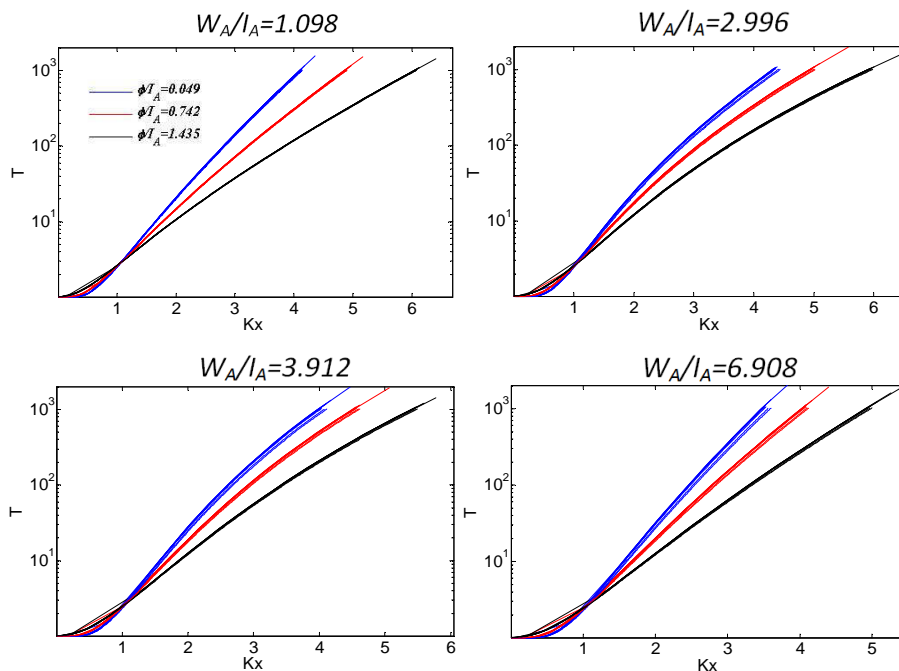
Fig. 1. Growth curves obtained for $r_L = 0.1$, $r_H = 0.3$, and different values of ϕ/I_A (as in the legend), I_1 (10, 50 mm h^{-1}), A (10, 50, 100, 200, 500 km^2), W_A/I_A (in subplots).

whose distribution is independent from the expected value, being obviously $E[K_x] = 1$. The growth curve depends on the coefficient of variation and on the skewness of the distribution. The TCIF arises as a distribution of annual maximum of a Poisson compound process, just as many other distributions of extreme values (e.g. GEV, TCEV). The coefficient of variation of such distributions mainly depends on the mean annual number of flood events Λ_q, and the TCIF distribution does not make an exception as it was confirmed by numerical investigation. Thus, the representation of TCIF growth curves characterized by the same value of Λ_q and different values of the other parameters allows the identification of shape changes on the growth curve, with direct reference to

the return period of the growth factor. The return period (defined as the inverse of the probability that a given event will be exceeded) is reported on the y-axis in a log scale limiting the range of values to those of technical interest (1–1000 yr).

Figures 1–5 display the TCIF growth curves obtained for different combinations of parameters. In all figures, TCIF growth curves are obtained for fixed values of r_L and r_H changing the parameters I_1, A, ϕ/I_A and W_A/I_A. Figures 1 and 2, which differ for the values of r_L and r_H ($r_L = 0.1$ and $r_H = 0.3$ in Fig. 1, $r_L = 0.1$ and $r_H = 0.9$ in Fig. 2), are divided in four subplots; each subplot reports the growth curves obtained for different values of I_1, A, ϕ/I_A and a fixed value of the ratio W_A/I_A (sample values are taken

Table 8. Mean and standard deviation of skewness for $r_L = 0.3$, $r_H = 0.9$; A ranges from 10 to 500 km^2 and I_1 ranges from 10 to 50 mm h^{-1}.

|	Mean of skewness					
	$W_A/I_A = 1.098$	$W_A/I_A = 2.302$	$W_A/I_A = 2.996$	$W_A/I_A = 3.912$	$W_A/I_A = 5.298$	$W_A/I_A = 6.908$
$\phi/I_A = 0.049$	1.472	1.692	1.696	1.638	1.570	1.544
$\phi/I_A = 0.742$	1.585	1.779	1.755	1.680	1.610	1.586
$\phi/I_A = 1.435$	1.784	1.935	1.885	1.799	1.730	1.707
	Standard deviation of skewness					
	$W_A/I_A = 1.098$	$W_A/I_A = 2.302$	$W_A/I_A = 2.996$	$W_A/I_A = 3.912$	$W_A/I_A = 5.298$	$W_A/I_A = 6.908$
$\phi/I_A = 0.049$	2.33E-03	5.16E-03	6.49E-03	7.62E-03	8.29E-03	8.51E-03
$\phi/I_A = 0.742$	1.85E-03	3.90E-03	4.76E-03	5.44E-03	5.80E-03	5.91E-03
$\phi/I_A = 1.435$	1.36E-03	2.80E-03	3.31E-03	3.64E-03	3.78E-03	3.83E-03
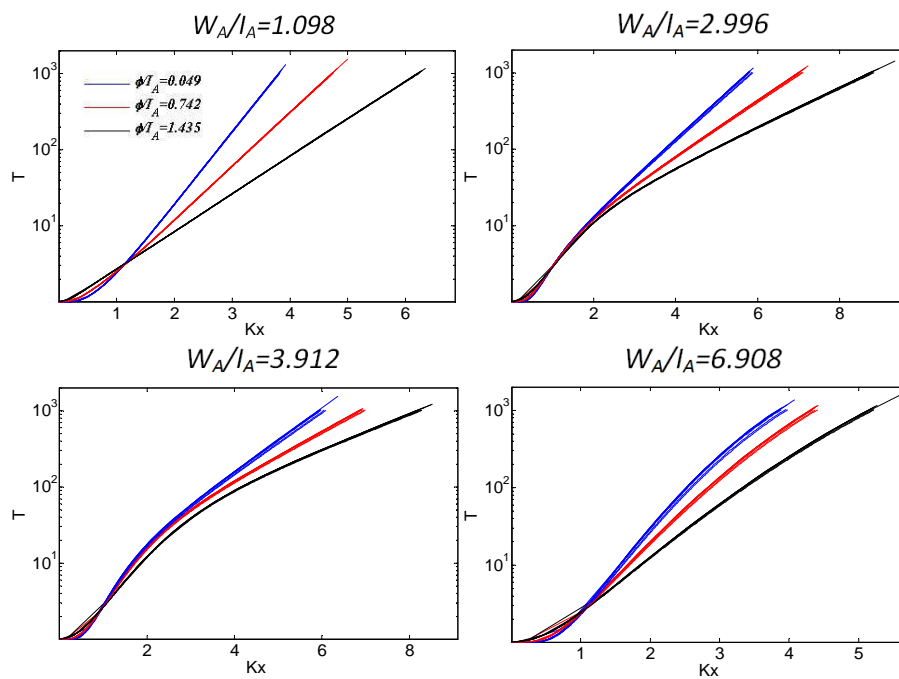
Fig. 2. Growth curves obtained for $r_L = 0.1$, $r_H = 0.9$, and different values of ϕ/I_A (as in the legend), I_1 (10, 50 mm h^{-1}), A (10, 50, 100, 200, 500 km^2), W_A/I_A (in subplots).

from the lower part of Table 4, first, third, fourth and sixth columns). We grouped by colour all cdfs with the same value of ϕ/I_A (i.e. with the same Λ_q and Coefficient of Variation): in blue $\phi/I_A = 0.049$ ($\Lambda_q = 20$), in red $\phi/I_A = 0.742$ ($\Lambda_q = 10$), in black $\phi/I_A = 1.435$ ($\Lambda_q = 5$). In each subplot, the three groups of cdfs differ in both the scale and the shape factor. As a first important evidence in Figs. 1 and 2, we observe that the TCIF cdfs obtained using different values of basin area A and rainfall intensity I_1, and keeping constant the ratios W_A/I_A and ϕ/I_A, practically collapse into one curve. Thus, in Tables 5–9, for a set of couples of r_L

and r_H values, ($r_L = 0.1$ and $r_H = 0.3$ in Table 5, $r_L = 0.1$ and $r_H = 0.6$ in Table 6, $r_L = 0.3$ and $r_H = 0.6$ in Table 7, $r_L = 0.3$ and $r_H = 0.9$ in Table 8, $r_L = 0.1$ and $r_H = 0.9$ in Table 9), we report the values of the coefficient of skewness of such TCIF cdfs obtained with fixed values of W_A/I_A and ϕ/I_A changing both the values of basin area $A = 10, 50, 100, 200, 500$ km^2 and of rainfall intensity $I_1 = 10, 50$ mm h^{-1}. Following the previous observation regarding the insensitivity of the coefficient of skewness to A and I_1, we report in each cell only the mean value and the standard deviation of the skewness coefficients of ten cdfs obtained by considering only the variability

Table 9. Mean and standard deviation of skewness for $r_L = 0.1$, $r_H = 0.9$; A ranges from 10 to 500 km^2 and I_1 ranges from 10 to 50 mm h^{-1}.

|	$W_A/I_A = 1.098$	$W_A/I_A = 2.302$	$W_A/I_A = 2.996$	$W_A/I_A = 3.912$	$W_A/I_A = 5.298$	$W_A/I_A = 6.908$
			Mean of skewness			
$\phi/I_A = 0.049$	1.400	2.130	2.729	3.346	3.096	2.097
$\phi/I_A = 0.742$	1.611	2.585	3.185	3.565	2.888	1.962
$\phi/I_A = 1.435$	1.994	3.144	3.662	3.723	2.761	1.966
			Standard deviation of skewness			
	$W_A/I_A = 1.098$	$W_A/I_A = 2.302$	$W_A/I_A = 2.996$	$W_A/I_A = 3.912$	$W_A/I_A = 5.298$	$W_A/I_A = 6.908$
$\phi/I_A = 0.049$	7.89E-03	2.37E-02	4.30E-02	8.60E-02	1.29E-01	7.67E-02
$\phi/I_A = 0.742$	6.01E-03	2.03E-02	3.78E-02	6.70E-02	6.33E-02	1.10E-02
$\phi/I_A = 1.435$	4.78E-03	1.82E-02	3.21E-02	4.53E-02	1.90E-02	2.11E-02
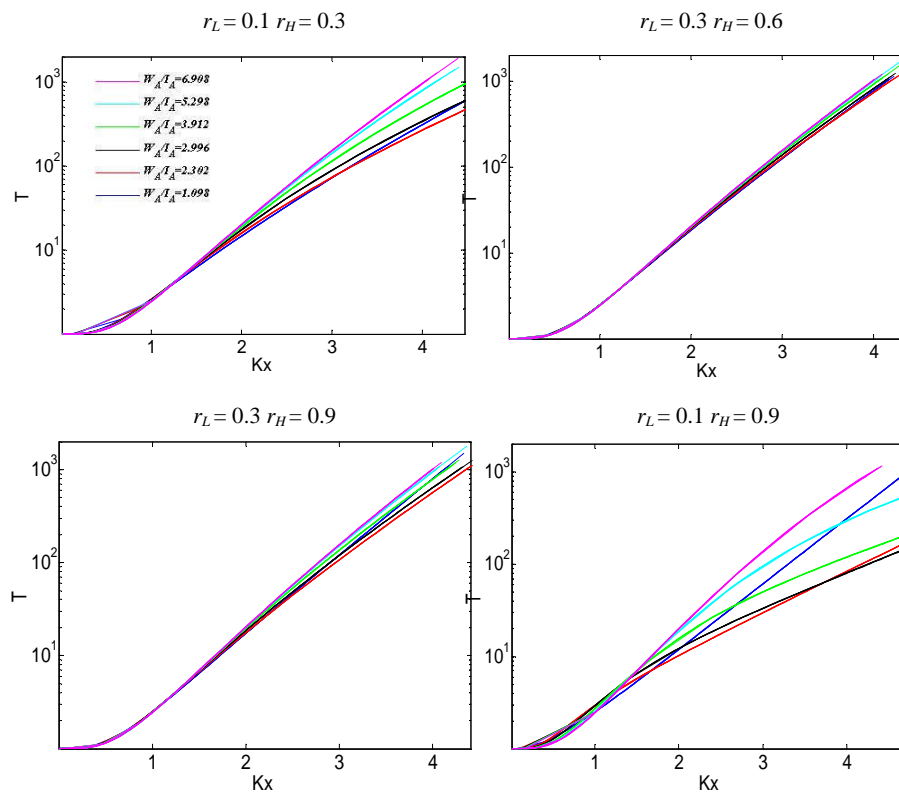
Fig. 3. Growth curves obtained for a constant value of ϕI_A (0.742), and varying W_A/I_A (as in the legend), I_1 (10, 50 mm h^{-1}), A (10, 50, 100, 200, 500 km^2), r_L and r_H (in subplots).

of basin area and rainfall intensity. The results show a standard deviation always significantly lower than the average coefficient of skewness.

Observing more carefully results reported in Tables 5–9, one may appreciate the effects of model parameters on skewness coefficient. In Table 5, for $r_L = 0.1$ and $r_H = 0.3$, the mean coefficient of skewness ranges from 1.608 to a maximum value of 2.452. In Table 6, for $r_L = 0.1$, $r_H = 0.6$, the

mean coefficient of skewness ranges from 1.595 to 3.417. In Table 7, for $r_L = 0.3$, $r_H = 0.6$ the mean coefficient of skewness ranges from 1.540 to 1.826, which is the minimum peak of skewness observed over all the parameter sets. In Table 8, for $r_L = 0.3$, $r_H = 0.9$, we observe the minimum coefficient of skewness equal to 1.472 and a peak of skewness of 1.935. In Table 9, for $r_L = 0.1$, $r_H = 0.9$ we have the minimum coefficient of skewness of 1.400 and a peak of skewness of 3.723,
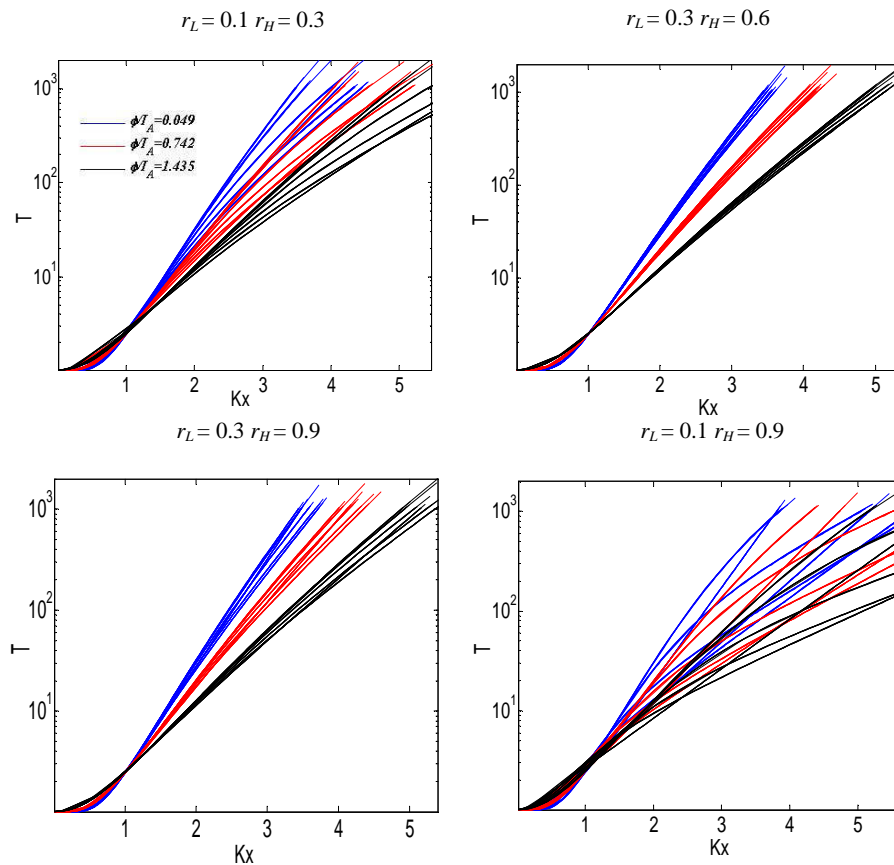
Fig. 4. Growth curves obtained varying ϕI_A (as in the legend), W_A/I_A (as in Table 4), I_1 (10, 50 mm h^{-1}), A (10, 50, 100, 200, 500 km^2), r_L and r_H (in subplots).

which is also the highest value observed over all the parameter sets. In general, comparing results of Tables 5–9, a strong relationship between skewness and ϕ can be observed. In fact, the minimum value of the coefficient of skewness is always observed for low values of ϕ and W_A that may be either low or high. On the other hand, a peak of skewness is always observed for medium values of W_A and for medium or high values of ϕ. In other words, the coefficient of skewness shows maximum values for medium-high values of the soil infiltration rate at saturation and medium values of soil storage capacity. It is important to highlight the consistency of these results with contents of Table 2. In fact, the skewness is high when both components of flood distribution affect the distribution of extreme flood events because they are not too low in order to be relevant and are not too rare in order to be observed. The skewness is low when only one component is relevant because either one of the two thresholds is low or the second threshold is high and exceedances are too rare to be observed.

In order to better understand the comparison among the different curves, accounting for both the scale factor and the shape factor effects, in Fig. 3 are reported different growth curves for four couples of r_L and r_H with a different

organization with respect to those reported in Figs. 1 and 2. In this case, each subplot reports different TCIF cdfs that have a fixed ratio ϕ/I_A and variable values of W_A/I_A (only curves for the medium value of ϕ/I_A are shown), I_1 and A. Obviously, even in these subplots the cdfs obtained for different values of I_1 and A collapse into one curve, but the colour code is used in order to identify different values of W_A/I_A. Since ϕ/I_A is fixed, in each of these subplots all curves have the same scale factor. Then the differences shown by the different values of W_A/I_A are all due to the curve shape factor, i.e. the coefficient of skewness. By comparing the four subplots of Fig. 3, one could notice that the minimum skewness is provided by a higher value of r_L (0.3). On the other hand, the largest scatter is observed with a low value of r_L (0.1) and a high r_H (0.9).

The TCIF cdfs obtained for different sets of parameters are also shown in Fig. 4, providing a complete overview of the effects due to the parameters I_1, A, W_A/I_A and ϕ/I_A. The scatter in the scale factor dominates subplots with a higher value of r_L (0.3), while in subplots with a lower value of r_L (0.1), the higher scatter in the shape factor produces cdfs with different scale factors with a marked overlap.

Table 10. Mean and standard deviation of skewness for different values of $r_L = r_H$; A ranges from 10 to 500 km^2 and I_1 ranges from 10 to 50 mm h^{-1}.

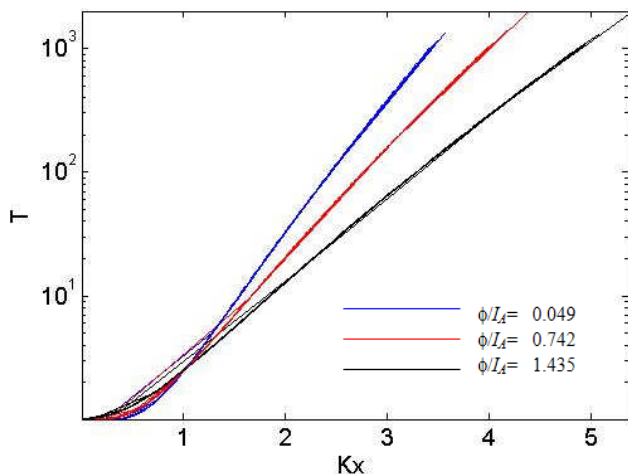|	$r_L = r_H = 0.05$			$r_L = r_H = 0.3$	
	Mean of skewness	Standard deviation of skewness		Mean of skewness	Standard deviation of skewness
$\phi/I_A = 0.049$	1.597	4.39E-02	$\phi/I_A = 0.049$	1.538	8.70E-03
$\phi/I_A = 0.742$	1.631	3.92E-02	$\phi/I_A = 0.742$	1.580	6.01E-03
$\phi/I_A = 1.435$	1.743	3.26E-02	$\phi/I_A = 1.435$	1.701	3.90E-03
	$r_L = r_H = 0.1$			$r_L = r_H = 0.9$	
	Mean of skewness	Standard deviation of skewness		Mean of skewness	Standard deviation of skewness
$\phi/I_A = 0.049$	1.574	2.92E-02	$\phi/I_A = 0.049$	1.235	3.16E-05
$\phi/I_A = 0.742$	1.579	1.94E-02	$\phi/I_A = 0.742$	1.264	7.07E-05
$\phi/I_A = 1.435$	1.684	3.74E-02	$\phi/I_A = 1.435$	1.377	7.38E-05

Fig. 5. Growth curves obtained for $r_L = r_H = 0.05$ and varying ϕ/I_A (as in the legend), W_A/I_A (as in Table 4), I_1 (10, 50 mm h^{-1}), A (10, 50, 100, 200, 500 km^2).

Fig. 6. Maximum skewness coefficient vs. r_H/r_L^2, for $\Lambda_p = 21$, $\varepsilon = 0.3$ (magenta) and $\Lambda_p = 21$, $\varepsilon = 0.4$ (blue).

For the same values of $\Lambda_p = 21$ and $\varepsilon = 0.3$, we report in Table 10 four cases obtained with $r_L = r_H = 0.05$, 0.1, 0.3 and 0.9. As shown in Fig. 5, relative to $r_L = r_H = 0.05$, all cdfs with the same value of ϕ/I_A and different values of I_1, A and also W_A/I_A collapse into one group of curves, with a practically null scatter. Other values of $r_L = r_H$ provide analogous behaviour. In this case the mean value and the standard deviation of the coefficients of skewness are evaluated on a set of 60 cdfs obtained, for any value of ϕ/I_A, by combining the ratios $W_A/I_A = 1.098, 2.302, 2.996, 3.912, 5.298, 6.908$ (as in bottom part of Table 4) with the values of basin area $A = 10, 50, 100, 200, 500$ km^2 and the rainfall intensities $I_1 = 10, 50$ mm h^{-1}. Also in this case the standard deviation is always significantly smaller than the average skewness. Results in Table 10 show that the skewness
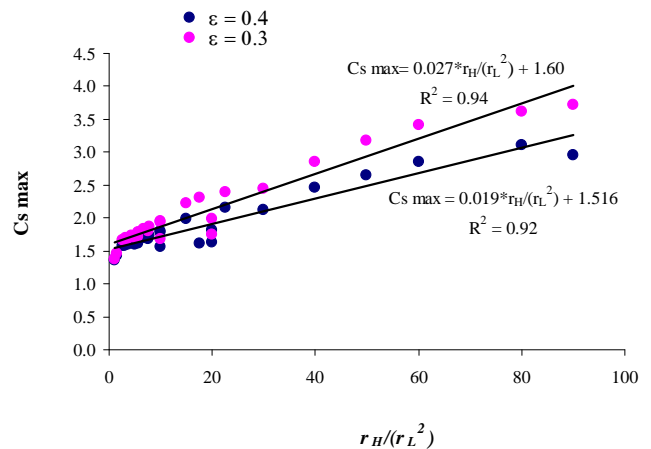
always grows with ϕ and higher skewness is obtained for lower values of $r_L = r_H$. The minimum value of the skewness is 1.235 and is obtained for the highest value of $r_L = r_H = 0.9$. This value, which is also the minimum value observed over the entire dataset of simulations, is not far from but significantly higher than the skeweness coefficient of a Gumbel distribution which is equal to 1.13955. Analogous evaluations were performed considering different values of Λ_p and ε, parameters that reflect, respectively, the rainfall coefficient of variation (Λ_p) and the average rainfall scaling with area (ε, see Eq. 6). In particular for $\Lambda_p = 75$ and $\varepsilon = 0.3$, $\Lambda_p = 21$ and $\varepsilon = 0.4$, and $\Lambda_p = 40$ and $\varepsilon = 0.4$: in all cases the results confirm the behaviour displayed for $\Lambda_p = 21$ and $\varepsilon = 0.3$.

By the analysis of the overall results obtained from the entire dataset of cdfs and related coefficients of skewness, we also found another important evidence: A strong relationship
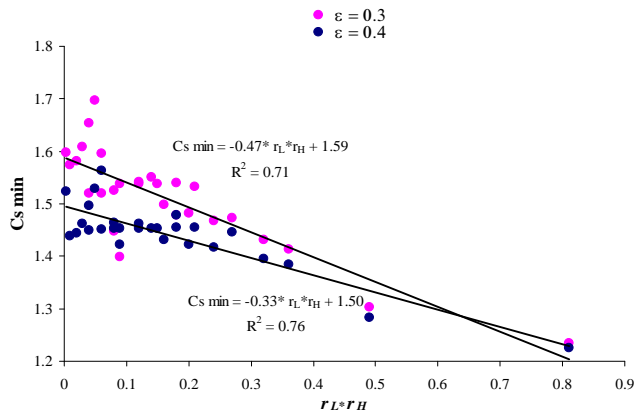
Fig. 7. Minimum skewness coefficient vs. $r_L \cdot r_H$ for $\Lambda_p = 21$, $\varepsilon = 0.3$ (magenta) and $\Lambda_p = 21$, $\varepsilon = 0.4$ (blue).

exists between the coefficient of skewness and the parameters r_L and r_H, independently from the variability of all other parameters. As we report in Fig. 6, the values of the maximum coefficient of skeweness, obtained for different values of r_L and r_H by varying the other parameters, show a strong linear dependence on the ratio r_H/r_L^2. On the other hand, Fig. 7 reports a dependence between the minimum coefficient of skewness and the product $r_H \cdot r_L$ obtained by varying I_1, A, W_A/I_A and ϕ/I_A. In Figs. 6 and 7 we also show results obtained for several other couples of r_L and r_H reported in Table 11.

5 Conclusions

The sensitivity analysis performed over parameters of the TCIF distribution provides interesting insights on the control that some physically-based parameters have on the skewness coefficient. The main results are summarized in the following:

1. the dimensionless ratios ϕ/I_A and W_A/I_A strongly affect the distribution skewness and the growth curve (Figs. 1–5);

2. for a fixed combination of the dimensionless ratios ϕ/I_A and W_A/I_A, the skewness coefficient is independent from the basin area A (ranging from 10 to 500 km^2), and rainfall intensity per unit area I_1 (ranging from 10 to 50 mm h^{-1}), in the range of variability investigated in this paper (Tables 5–10 and Figs. 1–5);

3. for a fixed combination of the dimensionless ratios ϕ/I_A and W_A/I_A, the skewness coefficient is also independent from Λ_p ranging from 21 to 75;

4. for a fixed combination of the dimensionless ratios ϕ/I_A and W_A/I_A, the skewness coefficient shows a

Table 11. Minimum and maximum skewness coefficient obtained for different values of r_L and r_H; for $\Lambda_p = 21$, and $\varepsilon = 0.3$ or $\varepsilon = 0.4$.

r_L	r_H	$\varepsilon = 0.3$		$\varepsilon = 0.4$	
		C_s max	C_s min	C_s max	C_s min
0.05	0.05	1.743	1.597	1.673	1.523
0.1	0.1	1.684	1.574	1.560	1.439
0.3	0.3	1.701	1.538	1.605	1.450
0.2	0.2	1.705	1.519	1.596	1.452
0.4	0.4	1.671	1.498	1.577	1.431
0.7	0.7	1.469	1.303	1.429	1.283
0.9	0.9	1.377	1.235	1.354	1.226
0.1	0.3	2.452	1.608	2.123	1.462
0.1	0.6	3.417	1.595	2.861	1.564
0.3	0.6	1.826	1.540	1.694	1.454
0.3	0.9	1.935	1.472	1.783	1.447
0.3	0.4	1.735	1.738	1.623	1.453
0.2	0.3	1.803	1.520	1.675	1.451
0.2	0.6	2.226	1.541	1.991	1.463
0.4	0.6	1.683	1.468	1.588	1.416
0.1	0.2	1.994	1.581	1.820	1.444
0.1	0.4	2.853	1.654	2.461	1.496
0.1	0.5	3.182	1.696	2.641	1.528
0.1	0.8	3.623	1.448	3.103	1.465
0.1	0.9	3.723	1.400	2.952	1.422
0.2	0.4	1.946	1.524	1.793	1.453
0.2	0.7	2.314	1.550	1.612	1.453
0.2	0.9	2.402	1.479	2.162	1.478
0.3	0.5	1.782	1.538	1.666	1.453
0.3	0.7	1.873	1.533	1.729	1.455
0.4	0.5	1.672	1.482	1.578	1.422
0.4	0.8	1.707	1.431	1.610	1.395
0.4	0.9	1.717	1.413	1.619	1.384

significant dependence on the rainfall scaling coefficient ε (Figs. 6 and 7);

5. in all cases, for fixed ϕ/I_A the skewness coefficient assumes a local maximum for increasing W_A/I_A (Tables 5–9 and Figs. 3–5);

6. if $r_L = r_H$, the skewness coefficient (C_s) is independent from W_A:$C_s = f(\phi/I_A)$ (Fig. 5);

7. if $r_L \neq r_H$, the skewness coefficient depends on both ϕ and W_A:$C_s = f(\phi/I_A, W_A/I_A)$ (Tables 5–9 and Figs. 1–4);

8. for a fixed value of Λ_p and ε, the maximum skewness increases with the ratio r_H/r_L^2 (Fig. 6);

9. for a fixed value of Λ_p and ε, the combination $r_L = r_H$ produces low values of skewness which also decreases with r_L (Table 10);

10. for a fixed value of Λ_p and ε, the minimum skewness decreases with the product $r_L \cdot r_H$ (Fig. 7).

The above presented sensitivity analysis was performed assuming rainfall as exponential distributed. Hence the rainfall annual maxima are Gumbel distributed and their coefficient of skewness is always equal to 1.13955. The resulting flood skew is always higher than this and it reaches its maximum values when the probability of observing two different runoff components is high. For this purpose it is necessary that the infiltration rate at saturation is not too high compared to average rainfall so that it is significant for developing an ordinary component, and it is also necessary that the soil storage is neither too low nor too high compared to average rainfall. In fact, if soil storage is too, low the second component is not distinguishable from the first component. If soil storage is too high, the second component becomes too rare and thus not significant for observable values. For fixed combination of other parameters and mainly r_L and r_H, by changing I_1, A, ϕ/I_A and W_A/I_A, it is possible to obtain a maximum value of C_s. Such a value is high as much as both r_L and r_L/r_H (Tables 5–10, Figs. 1–3) decrease, thus C_s shows a straight relationship with r_H/r_L^2 (Fig. 6). On the other hand, the minimum values of C_s are obtained, independently from the values of ϕ/I_A and W_A/I_A, when $r_L = r_H$ (Table 10 and Fig. 5). In such a case there is no evidence of the second component. The condition $r_L = r_H$ can be obtained in real basins for geomorphological reasons, for example, when valleys are very steep and the average contributing area is always low. In such a case we may have two significant components but a skewness coefficient not very high. Further research is needed for the case $k \neq 1$, i.e. when rainfall is not exponential distributed and may assume high skewness coefficient. In such a case a strong flood skewness could be expected even for single component runoff mechanisms.

Our results indicate that a strong role is played by storage effects, as observed by McCuen and Smith (2008); nevertheless we observe that by introducing two different runoff thresholds, flood skew may also reach much higher values than rainfall skew.

Such considerations could provide precious source of information when dealing, for example, with flood frequency regional analysis. In fact, it is widely accepted that the investigation of regional statistical homogeneity should be searched according to hydrologic similarity, but the same concept of hydrologic similarity is not completely defined and universally cleared. As a result, often the search for homogeneous areas reduces to a trial-and-error exercise. The final considerations listed above in points 1 to 5 provide quantitative indications about the dependence of the coefficient of skewness from quantities related to rainfall and soil properties which are useful for the investigation of spatial variability of C_s.

On the other hand, considerations listed in points 6 to 10 provide interesting possibility of investigation about the role played by the distribution of contributing areas according to different mechanisms of runoff generation. We believe that, while the basic concepts of source area models have been proposed for years (e.g. Troendle, 1985), the practical application of models based on this promising phenomenological description of the flood generation process is not fully developed. The TCIF distribution, as well as other derived distributions based on the concept of partial contributing area, could provide a complete framework for exploiting such kind of information about hydrological regime and basin response. Nevertheless, while we believe that a strong role is played by basin morphology, there is still an open field of investigation on the ways for estimating these distribution variables in ungauged basins.

List of model parameters, units and short description.

A (km^2)	basin area;
a_L	L-type (frequent) source area contributing to runoff peak
a_H	H-type (rare) source area contributing to runoff peak
$\tau(h)$	lag-time of contributing area
ξ	routing factor
β	scale parameter of Gamma distribution
$E[i_{A,\tau}] = I_A$ (mm h^{-1})	average rainfall intensity referred to the entire basin area A
I_1 (mm h^{-1})	rainfall intensity per unit contributing area
ε	scale parameter of the relationship between average rainfall intensity $E[i_{a,\tau}]$ and source area a
Λ_p	mean annual number of independent rainfall events
k	shape parameter of the Weibull distribution of the rainfall intensity
Λ_q	mean annual number of independent flood events
$f_{A,L}$ (mm h^{-1})	lower runoff threshold referred to the entire basin area A
$f_{A,H}$ (mm h^{-1})	higher runoff threshold referred to the entire basin area A
ε_L	scale parameter of the relationship between average hydrologic loss ($f_{a,L}$) and source area a

ε_H	scale parameter of the relationship between average hydrologic loss ($f_{a,H}$) and source area a
r_L	ratio of the L-type mean contributing area $E[a_L]$ to the total basin area A
r_H	ratio of the H-type mean contributing area $E[a_H]$ to the total basin area A
Λ_L	mean annual number of independent flood events for L-type
Λ_H	mean annual number of independent flood events for H-type
C_s	skewness coefficient
C_v	coefficient of variation
$u_{a,L}$ (mm h^{-1})	L-type (frequent) peak unit runoff
$u_{a,H}$ (mm h^{-1})	H-type (rare) peak unit runoff
q_o (m^3 s^{-1})	base flow
q_p (m^3 s^{-1})	annual maximum flood peak
CDF$_{Qp}(q_p)$	cumulative probability distribution of the annual maximum flood peak
PDF$_{Qp}(q_p)$	probability density function of the annual maximum flood peak
ϕ (mm h^{-1})	spatial average of soil infiltration rate in saturated conditions
W_A (mm h^{-1})	soil water storage capacity averaged in space and over the basin lag-time
α_L	position parameter of the gamma distribution of the L_Type contributing area to flood peak
α_H	position parameter of the gamma distribution of the H_Type contributing area to flood peak

Edited by: P. A. Troch

References

Beven, K. J.: Towards the use of catchment geomorphology in flood frequency predictions, Earth Surf. Proc. Land., 12, 6–82, 1987.

Blazkova, S. and Beven, K. J.: Flood frequency estimation by continuous simulation for a catchment treated as ungauged (with uncertainty), Water. Resour. Res., 8, 1–14, 2002.

Blazkova, S. and Beven, K.: Flood frequency estimation by continuous simulation of subcatchment rainfalls and discharges with the aim of improving dam safety assessment in a large basin in the Czech Republic, J. Hydrol., 292, 153–172, 2004.

Bocchiola, D. and Rosso, R.: Use of a derived distribution approach for flood prediction in poorly gauged basins: A case study in Italy, Adv. Water Resour., 32, 1284–1296, 2009.

De Michele, C. and Salvadori, G.: On the derived flood frequency distribution: analytical formulation and the influence of antecedent soil moisture condition, J. Hydrol., 262, 245–258, 2002.

Eagleson, P. S.: Dynamics of flood frequency, Water Resour. Res., 8, 878–898, 1972.

Fiorentino, M. and Iacobellis, V.: New insights about the climatic and geologic control on the probability distribution of floods, Water Resour. Res., 37, 721–730, 2001.

Fiorentino, M., Gabriele, S., Rossi, F., and Versace, P.: Hierarchical approach for regional flood frequency analysis, in: Regional flood frequency analysis, edited by: Singh, V. P., D. Reidel, Norwell, Mass, 35–49, 1987.

Fiorentino, M., Manfreda, S., and Iacobellis, V.: Peak runoff contributing area as hydrological signature of the probability distribution of floods, Adv. Water Resour., 30, 2123–2134, 2007.

Fiorentino, M., Gioia, A., Iacobellis, V., and Manfreda, S.: Regional analysis of runoff thresholds behaviour in Southern Italy based on theoretically derived distributions, Adv. Geosci., 26, 139–144, doi:10.5194/adgeo-26-139-2011, 2011.

Franchini, M., Galeati, G., and Lolli, M.: Analytical derivation of the flood frequency curve through partial duration series analysis and a probabilistic representation of the runoff coefficient, J. Hydrol., 303, 1–15, 2005.

Gioia, A., Iacobellis, V., Manfreda, S., and Fiorentino, M.: Runoff thresholds in derived flood frequency distributions, Hydrol. Earth Syst. Sci., 12, 1295–1307, doi:10.5194/hess-12-1295-2008, 2008.

Gottschalk, L. and Weingartner, R.: Distribution of peak flow derived from a distribution of rainfall volume and runoff coefficient, and a unit hydrograph, J. Hydrol., 208, 148–162, 1998.

Iacobellis, V. and Fiorentino, M.: Derived distribution of floods based on the concept of partial area coverage with a climatic appeal, Water Resour. Res., 36, 469–482, 2000.

Iacobellis, V., Claps, P., and Fiorentino, M.: Climatic control on the variability of flood distribution, Hydrol. Earth Syst. Sci., 6, 229–238, doi:10.5194/hess-6-229-2002, 2002.

Iacobellis, V., Gioia, A., Manfreda, S., and Fiorentino, M.: Flood quantiles estimation based on theoretically derived distributions: regional analysis in Southern Italy, Nat. Hazards Earth Syst. Sci., 11, 673–695, doi:10.5194/nhess-11-673-2011, 2011.

Kusumastuti, D. I., Struthers, I., Sivapalan, M., and Reynolds, D. A.: Threshold effects in catchment storm response and the occurrence and magnitude of flood events: implications for flood frequency, Hydrol. Earth Syst. Sci., 11, 1515–1528, doi:10.5194/hess-11-1515-2007, 2007.

Loukas, A.: Flood frequency estimation by a derived distribution procedure, J. Hydrol., 255, 69–89, 2002.

Matalas, N. C., Slack, J. R., and Wallis, J. R.: Regional skew in search of a parent, Water Resour. Res., 11, 815–826, 1975.

McCuen, R. H. and Smith, E.: Origin of Flood Skew, J. Hydrol. Eng.-ASCE, 13, 771–775, doi:10.1061/(ASCE)1084-0699(2008)13:9(771), 2008.

McGrath, G. S., Hinz, C., and Sivapalan, M.: Temporal dynamics of hydrological threshold events, Hydrol. Earth Syst. Sci., 11, 923–938, doi:10.5194/hess-11-923-2007, 2007.

Merz, R. and Bloschl, G.: A regional analysis of event runoff coefficients with respect to climate and catchment characteristics in Austria, Water Resour. Res., 45, W01405, doi:10.1029/2008WR007163, 2009.

NERC – Natural Environment Research Council: Flood studies report, Vol. I – Hydrologic studies, NERC, London, 1975.

Raines, T. H. and Valdes, J. B.: Estimation of flood frequencies for ungauged catchments, J. Hydrol. Eng.-ASCE, 119, 1138–1154, 1993.

Sivapalan, M., Wood, E. F., and Beven, K. J.: On hydrologic similarity, 3, A dimensionless flood frequency model using a generalized geomorphologic unit hydrograph and partial area runoff generation, Water Resour. Res., 26, 43–58, 1990.

Strupczewski, W. G., Kochanek, K., Markiewicz, I., Bogdanowicz, E., Weglarczyk, S., and Singh, V. P.: On the tails of distributions of annual peak flow, Hydrol. Res., 42, 171–192, 2011.

Struthers, I. and Sivapalan, M.: A conceptual investigation of process controls upon flood frequency: role of thresholds, Hydrol. Earth Syst. Sci., 11, 1405–1416, doi:10.5194/hess-11-1405-2007, 2007.

Troendle, C. A.: Variable source area models, in: Hydrological Forecasting, edited by: Anderson, M. G. and Burt, T. P., John Wiley & Sons Ltd., 1985.